CRYSTAL GROWTH & DESIGN

Communication

Cite This: Cryst. Growth Des. 2019, 19, 3085−3091

pubs.acs.org/crystal

High-Quality GaAs Planar Coalescence over Embedded Dielectric Microstructures Using an All-MBE Approach

Daniel J. Ironside,*[,†] Alec M. Skipper,[†] Thomas A. Leonard,[†] Marina Radulaski,[‡] Tomas Sarmiento,[‡] Pankul Dhingra,[¶] Minjoo L. Lee,[¶] Jelena Vučković,[‡] and Seth R. Bank*[,†]

[†]Department of Electrical and Computer Engineering, The University of Texas at Austin, Austin, Texas 78712, United States

[‡]E. L. Ginzton Laboratory, Stanford University, Stanford, California 94305, United States

[¶]Micro and Nanotechnology Lab, University of Illinois Urbana−Champaign, Urbana, Illinois 61801, United States

We demonstrate for the first time an entirely molecular beam epitaxy (MBE) approach to high-quality GaAs planar coalescence over embedded dielectric microstructures. Specifically, an all-MBE approach was achieved by developing a new two-stage growth process, merging the MBE growth regimes of III-flux modulated lateral epitaxial overgrowth (LEO) with self-ordered planarization of nonplanar substrates to produce highly selective planar coalescence specifically for embedding [010]-aligned silica gratings patterned on (001) substrates. The resulting planar coalescence returned a smooth (001) surface with surface roughness as low as 3 nm root-mean-square and photoluminescence (PL) equivalent to grating-free controls. In demonstrating high-quality GaAs coalescence, we also report for the first time an intentionally enhanced single InGaAs/GaAs/AlAs quantum well PL test structure seamlessly grown directly above embedded silica gratings, leading to a 1.4× enhancement in PL as a result of both Purcell and extraction enhancements corroborated by time-resolved PL studies. As a result, we provide a significant advance to the long-standing challenge of marrying high-quality semiconductor crystal growth with dielectric microstructures, unlocking several high-impact applications, such as enhanced quantum emitters and embedded metasurfaces for quantum information processing, and provide a pathway for all-MBE metamorphic III−V heteroepitaxy.

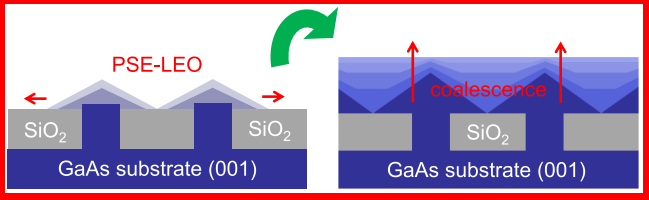

INTRODUCTION

Seamless integration of embedded dielectric microstructures in III−V crystal growth is an active area of research due to its numerous important applications. Recent efforts include increased light extraction via air voids in the III-Nitrides,[1,2] site-control of quantum emitters,[3,4] embedded air holes to create 2D-slab and 3D photonic crystals to enhance emitters,[5,6] and, most commonly, dislocation blocking in metamorphic heteroepitaxy for low defect III−V growth.[7−9] From an epitaxial growth perspective, the primary challenge in embedding dielectric microstructures is achieving single-crystal high-quality planar coalescence, which requires the joining of two or more crystal fronts without forming defects and returning the growth front to the substrate orientation, commonly the (001) plane. Since the challenges are growth-based, investigation into planar coalescence focuses entirely around the methodologies of a specific crystal growth technique. Planar coalescence for conventional III−V crystal growth over dielectric microstructures has been achieved for homoepitaxial liquid phase epitaxy (LPE)[10] and metal−organic vapor phase epitaxy (MOVPE)[11−14] in both homoepitaxial and metamorphic systems in large part due to liquid and/or gas phase precursors forming limited III−V polycrystalline nuclei on inert dielectric surfaces.

While prevalent in III−V crystal growth, solid-source MBE has a well-known "coalescence problem", historically lacking approaches for high-quality lateral epitaxial overgrowth and planar coalescence over micron-scaled dielectric structures,[15,16] in large part due to low diffusion of III-adatoms on dielectric surfaces, typically below 300 nm,[17] readily forming polycrystalline deposition on dielectric surfaces exceeding a diffusion length. Several solid-source MBE highly selective growth and/or LEO growth approaches have been reported;[18−20] however, no reported techniques have demonstrated LEO with planar coalescence.

To this end, in this Communication, we demonstrate for the first time an all-MBE growth approach for planar coalescence over embedded dielectric microstructures. Specifically, an all-MBE approach was achieved by developing a new two-stage growth process, merging the MBE growth regimes of III-flux modulated lateral epitaxial overgrowth (LEO) with self-ordered planarization of nonplanar substrates to produce highly selective planar coalescence specifically for embedding [010]-aligned silica gratings patterned on (001) substrates. The resulting planar coalescence returned a smooth (001) surface with surface roughness as low as 3 nm root-mean-square. As a sensitive probe to the crystal quality, an InGaAs/GaAs/AlAs quantum well (QW) photoluminescence test structure was grown directly above the embedded dielectric gratings after planar coalescence; the QW exhibited com-

Received: November 7, 2018
Revised: February 20, 2019
Published: April 10, 2019

DOI: 10.1021/acs.cgd.8b01671
Cryst. Growth Des. 2019, 19, 3085−3091

parable emission when compared to grating-free controls. To illustrate the utility of this new growth approach, we demonstrated that it is possible to tailor these structures to enhance emission of the PL test emitter. In particular, we observed a 1.4× enhancement to photoluminescence from test emitter grown directly above embedded 1.4 μm pitch silica gratings, resulting from a combination of Purcell and extraction enhancements. More specifically, this result marks the first enhancement of an emitter from embedded dielectric microstructures integrated using an entirely seamless growth approach. This represents a significant advance to the long-standing challenge of marrying high-quality semiconductor crystal growth with dielectric microstructures, unlocking several high-impact applications, including enhanced quantum emitters and embedded metasurfaces for quantum information processing, as well as an all-MBE approach to metamorphic III−V heteroepitaxy, all of which require a seamless integration of high-quality crystalline semiconductors and patterned dielectrics.

RESULTS AND DISCUSSION

While several approaches have extended highly selective LEO to MBE growth,[19,21,22] no reports of planar coalescence over embedded dielectric microstructures have been reported using a singular growth technique within MBE. Many MBE implementations achieve some degree of LEO including nonplanar lateral coalescence;[18,20] however, no singular growth technique within MBE has realized coalescence which returns the LEO to the substrate orientation, generally the (001) orientation. Instead, we introduce a two-stage growth approach to planar coalescence within an entirely MBE growth process. As depicted in Figure 1a,b, by identifying an MBE-based nonplanar LEO growth to encapsulate dielectric microstructures, a secondary MBE growth method can be employed to return the growth front through planarization,[23] essentially treating nonplanar LEO growth as a corrugated substrate. Under the proposed two-stage approach, a lateral growth mode must be identified such that nonplanar growth achieves well-defined facets of the fast surface diffusion variety, such as the (111)B or (011) family, as planarization can be achieved through capillary growth in the valleys.[23] Thus, an investigation of the lateral growth space was necessary to identify an MBE-based LEO growth system suitable for planarization.

As seen in Figure 1c, in the investigation of a two-stage all-MBE growth approach to embedded dielectric microstructures, key materials and growth variables were identified. A prototype material system was chosen as silica gratings embedded in GaAs epitaxial growth on (001) GaAs substrates. Silica was the preferential dielectric due to its chemical stability at conventional III−V MBE growth conditions and GaAs was chosen as the preferential III−V test material due to its wide growth space as well as its well-reported highly selective growth on masked silica substrates.[22,24,25] Since the integration of dielectric structures exceeding the Ga adatom diffusion lengths on silica was the goal, grating bar widths were varied at 0.7 μm, 0.8 μm, and 0.9 μm, all exceeding a Ga diffusion length by 2−3×.[17] To keep the methodology simple, the grating fill factor was fixed at 50%, resulting in grating pitches of 1.4 μm, 1.6 μm, and 1.8 μm, respectively. Finally, since GaAs growth is highly anisotropic with lateral growth preferred along the [1$\bar{1}$0] direction,[26] three grating alignments were varied, individually aligned to the [110], [010], and [1$\bar{1}$0] directions, respectively.

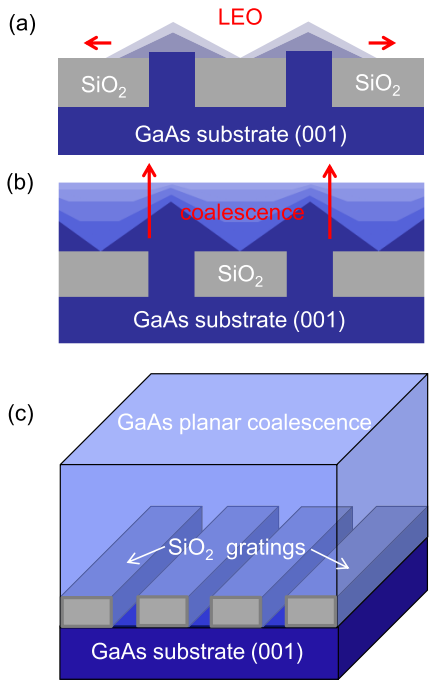

Figure 1. Cross-section illustration depicting the two-stage growth process by first (a) producing well-faceted LEO over dielectric microstructures to form a nonplanar template and (b) returning the templated LEO growth toward a planar episurface. (c) 3D drawing depicting the test material system: silica gratings embedded in GaAs.

Thus, in total, nine grating pitch and alignments were investigated.

To determine an MBE approach to produce a nonplanar LEO template, a growth spaces investigation was performed analyzing previously reported highly selective LEO techniques using the GaAs/SiO_2 test system. Among the investigated techniques, the most promising approach for LEO suitable to produce planar coalescence was identified as III-flux modulated MBE technique known as using Periodic Supply Epitaxy (PSE).[20,22,27] Using PSE growth, GaAs diffusion lengths on silica surfaces are extended from 300 nm under continuous conventional MBE growth to nearly 60 μm using the PSE growth approach,[22] sufficiently high for dielectric integration at the micron scale. More importantly, using PSE, we were able to demonstrate embedded grating systems which generate nonplanar LEO with fast surface diffusion facets and at high selectivity suitable for planarization, the result of which can be seen in Figure 2.

From the initial LEO investigation using the PSE approach, distinct differences emerged entirely dependent on the alignment of the gratings with respect to crystal direction and independent of grating pitch and bar width. Gratings aligned parallel to the [110] direction had significant LEO as seen in Figure 2a,b, emerging as {111}B faceted growth, consistent with MBE-GaAs growth on [110]-oriented mesas.[28] However, as the LEO progressed over the silica surface, nodules of dissimilar facets clearly emerged the edges of the {111}B lateral overgrowth after 180 cycles as seen in Figure 2a, and when further pushed to 360 cycles, its formation appeared to result in uneven lateral coalescence as seen in Figure 2b. While successful at generating LEO with fast diffusing facets,

DOI: 10.1021/acs.cgd.8b01671
Cryst. Growth Des. 2019, 19, 3085−3091

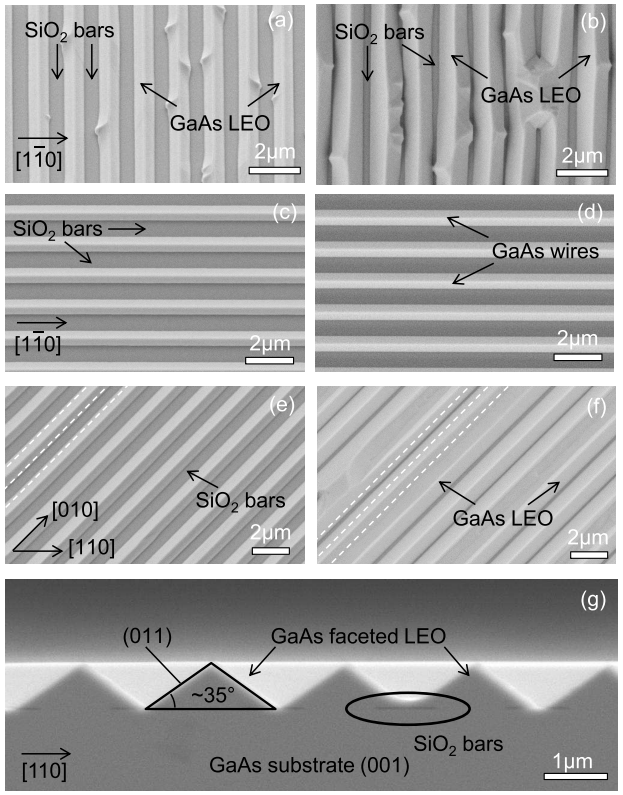

Figure 2. Planview SEM of GaAs LEO over 700 nm silica bars (a)−(f). Gratings aligned to [110] direction show uneven LEO for (a) 180 and (b) 360 PSE cycles. Gratings aligned along the [1$\bar{1}$0] direction show vertical growth for (c) 180 and (d) 360 PSE cycles. Gratings aligned along the [010] direction show well-faceted, uniform LEO for (e) 180 and (f) 360 PSE cycles. (g) After 360 cycles, gratings aligned along the [010] direction show the formation of {011}-faceted LEO and lateral coalescence. Representative dashed lines are placed to view the location of embedded silica gratings.

the uneven lateral coalescence from [110]-aligned gratings was marked as unsuitable for returning the nonplanar LEO to coalesce into a planar (001) surface.

For gratings aligned parallel to the [1$\bar{1}$0] direction, limited LEO was observed in contrast to previous reports, resulting in mostly vertical growth as seen in Figure 2c,d. Even after 360 cycles of PSE-GaAs growth, limited LEO was observed, forming {110} faceted sidewalls. This is consistent with preferred lateral growth for MBE-GaAs along the [1$\bar{1}$0] direction, and unsurprisingly in this demonstration, preferring growth within the windows, parallel to the gratings and limited LEO from forming across the silica surfaces. As such, the lack of lateral coalescence marks the [1$\bar{1}$0]-aligned gratings unsuitable for returning the growth to planar coalescence.

For gratings aligned parallel to the [010] direction, PSE LEO produces the most uniform and well-faceted PSE-LEO as seen in Figure 2e,f. As the LEO progressed over the silica surface, smooth {011}-faceted growth clearly emerged after 180 cycles as seen in Figure 2a and consistent with MBE-GaAs growth on [010]-oriented mesas.[14] When further pushed to 360 cycles, its formation appeared to result in partial lateral coalescence as seen in Figure 2f. Looking at cross-sectional SEM in Figure 2g, after 360 cycles, PSE-LEO clearly forms {011} facets, a preferred geometry due to its nearly 3:1 lateral to vertical growth along the [110] direction as well as fast surface diffusion.[29] Due to the smooth, well-faceted {011} LEO as well as partial lateral coalescence, [010]-aligned gratings were marked as the preferred growth space for returning the PSE-based LEO into planar coalescence through planarization.

With a fast-diffusing, {011}, well-faceted nonplanar LEO template growth space identified, investigation into planar coalescence through planarization was enabled. From work on planarization of corrugated substrate by Kapon et al.,[23,30] tailored continuous growth methods were identified as preferred for planarization as high diffusion valleyed structures to growth via "capillary" growth modes to return the nonplanar surface to the (001) substrate orientation. To investigate the second-stage growth dynamics of planarization under the proposed two-stage methodology, silica gratings were initially templated with GaAs LEO over [010]-aligned 1.4−1.8 μm pitch gratings using the previously described PSE method. In investigation of optimal LEO growth to promote smooth planarization, lateral growth achieving lateral coalescence solely through PSE growth was found to inhibit planarization as localized inhomogeneous growth containing a mixture of dissimilar facets emerged near the points of coalescence. This is evident for lateral growth of [110]-aligned and, to a lesser degree, [010]-aligned gratings as imaged in Figure 2b,f.

Instead, smooth planarization was found to occur when terminating lateral growth using PSE once the lateral separation achieved a distance less than a conventional Ga adatom diffusion length, then transitioning to continuous growth. In demonstration, 300 cycles of PSE under the aforementioned lateral growth conditions was performed, resulting in 100, 200, and 300 nm lateral growth separation for 700, 800, and 900 nm bar widths, respectively. In practice, a one-size-fits-all lateral growth approach is not necessary, but rather solely needed for this material investigation to maintain the same MBE growth environmental quality across all three samples. After the PSE lateral growth steps, continuous growth was performed until signs of planarization occurring from in situ reflective high-energy electron diffraction (RHEED) showed a streaky 2× pattern that became brighter with additional growth, indicating a smooth growth surface as seen in Figure 3a. This resulted in a total of 2 μm of additional growth to achieved a planar (001) episurface. Planarization of the LEO template occurred with a high degree of smoothness characterized ex situ. From visual inspection, the growth front regained a mirror-like appearance. Using cross-sectional SEM, silica grating can be plainly seen embedded in the GaAs overgrowth from the two-stage growth method as seen in Figure 3b owing to its contrast difference. Also, the planar (001) GaAs episurface above the embedded silica grating is evident.

The smoothness of the regained (001) GaAs surface after planarization was measured using atomic force microscopy (AFM) scans. Surface roughness after planar coalescence remained low but varied depending on the pitch of the samples. For the embedded 1.4−1.8 μm pitch samples, root-mean-square (RMS) surface roughness achieving a range between 3.2 and 7.2 nm RMS as plotted in Figure 3c. A clear exponential trend emerged as the surface roughness versus grating pitch, in agreement with previous modeling.[31] Also, the trendline allowed for a projection to sub-1 nm RMS roughness occurring for 0.8 μm pitch gratings at a 50% fill factor. Further surface roughness reduction may also occur for additional

DOI: 10.1021/acs.cgd.8b01671
Cryst. Growth Des. 2019, 19, 3085−3091

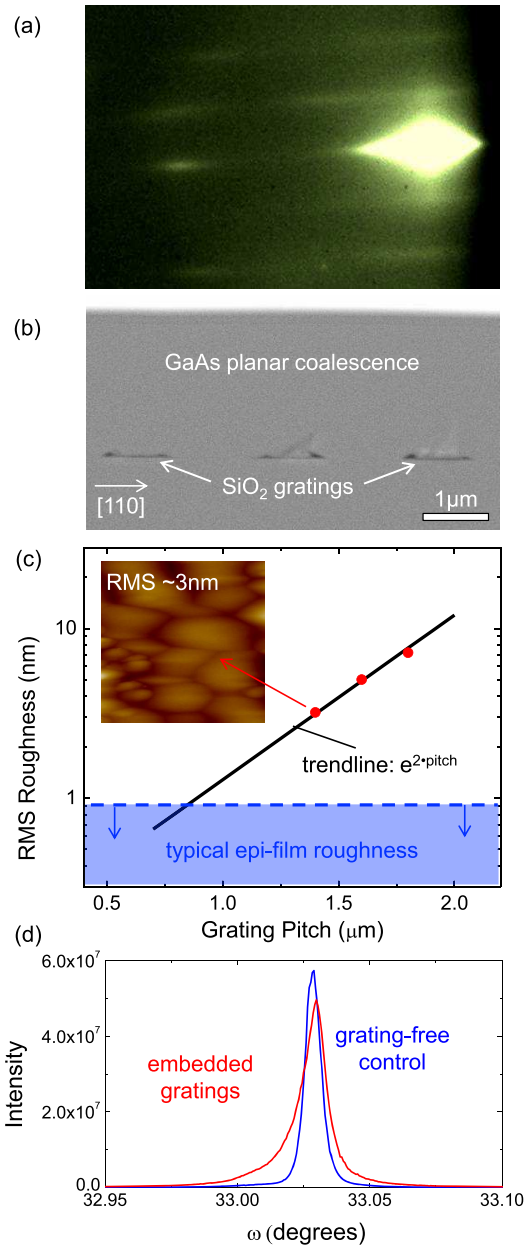

Figure 3. (a) RHEED image showing a clear 2× pattern after planarization. (b) Cross-sectional SEM of embedded silica gratings in GaAs overgrowth using the two-stage approach. (c) Plot of surface roughness varying grating pitch, which fits well to trendline projecting sub-1 nm roughness for 0.8 μm pitch gratings; the AFM inset shows the surface morphology of a 10 μm × 10 μm scan for the embedded 1.4 μm pitch gratings with 3.2 nm RMS surface roughness. (d) Comparable X-ray rocking curves between 1.4 μm pitch grating sample and grating-free control.

continuous growth and/or use of growth surfactants, such as Bi.[32,33]

While regaining the (001) surface within a few monolayers of roughness was promising, an investigation into material quality of the overgrown filmn using X-ray diffraction (XRD), electron channeling contrast imaging (ECCI), and photoluminescence spectroscopy (PL) was performed. In the initial characterization of coalescent films over embedded gratings, ECCI was performed over 10 μm × 10 μm regions. Limited threading dislocations were observed in these regions, suggesting dislocation densities below 10^6 cm^{-2}. The low defect density of the coalescent overgrowth films was also supported from XRD through rocking curve measurements around the GaAs (004) reflection as seen in Figure 3d. Compared to grating-free GaAs controls, some slight broadening was observed in overgrown films above grating regions with a fwhm of 19.9 arc seconds compared to the grating-free control region at a fwhm of 14.95 arc seconds. From Tartaglia et al., previous work has shown the relationship between XRD fwhm and etch pit density measurements of GaAs.[34] Based on their correlation, a defect density in the range of 10^4–10^6 cm^{-2} for fwhm's between 10.4 and 19.4 arc seconds was estimated for embedded grating samples, further confirming the defect density estimate from ECCI. Importantly, from the ECCI and XRD analysis, it suggests that the coalescence avoids the defect generating "two-zipper"-like coalescence, which would be generated over 10^7 cm^{-2} in density based on the grating pitch and bar width embedded in this investigation.

Thus, to better characterize the overgrowth, photoluminescence investigations were performed owing to its sensitivity to material defects, such as dislocations, at low densities. As an indicator of coalescence quality, an optical-pumped PL test emitter was grown after planar coalescence, composing of a single 10 nm $In_{0.15}Ga_{0.85}As$/GaAs quantum well (QW), 200 nm GaAs absorbing region sandwiched between two 10 nm AlAs wide band gap carrier blocking layers, electrically isolating the photogenerated carriers to the quantum well instead of alternate nonradiative recombination sites such as surface state or the silica/substrate interface. Thus, the test emitter gauges any reduction in PL as a result of nonradiative material defects from coalescence such as threading dislocations, point defects, and/or grain boundaries. Also, as a control, an identical emitter was grown on unpatterned grating-free (001) GaAs substrates using equivalent layer thicknesses including a 2.6 μm buffer layer. Finally, a large 80 μm spot size laser was used to probe material quality over several pitch widths.

From an initial investigation at room-temperature conditions, all embedded grating samples exhibited peak PL response within 2× compared to the grating-free control as seen in Figure 4a. The equivalent degree of luminescence of the material above embedded gratings compared to control strongly confirms that the planar coalescence from the two-stage growth approach is without significant nonradiative defects and that coalescence likely occurs as a "one-zipper"-like mode as opposed to the dislocation creating "two-zipper" mode,[35] the latter case resulting in a several orders of magnitude PL reduction. Also, two-stage MBE planar coalescence is in agreement with planar coalescence in MOVPE which observed equivalent dislocation-free coalescence for [010]-aligned dielectric structures[12] as characterized by TEM.

As a consequence of the PL material quality investigation, a significant increase in peak PL occurred for the emitter grown above the 1.4 μm pitch embedded gratings demonstrating 1.4× increase compared to control. As such, additional studies were undertaken to clarify the cause(s) of the increase. Excitation-dependent PL was performed on both the embedded 1.4 μm pitch gratings and control emitters to determine if the enhancement was due to high pumping intensities employed in the initial investigation. As seen in Figure 4b, the peak PL emission normalized to the control remained largely unchanged over a 2 orders of magnitude variation in pump

DOI: 10.1021/acs.cgd.8b01671
Cryst. Growth Des. 2019, 19, 3085−3091

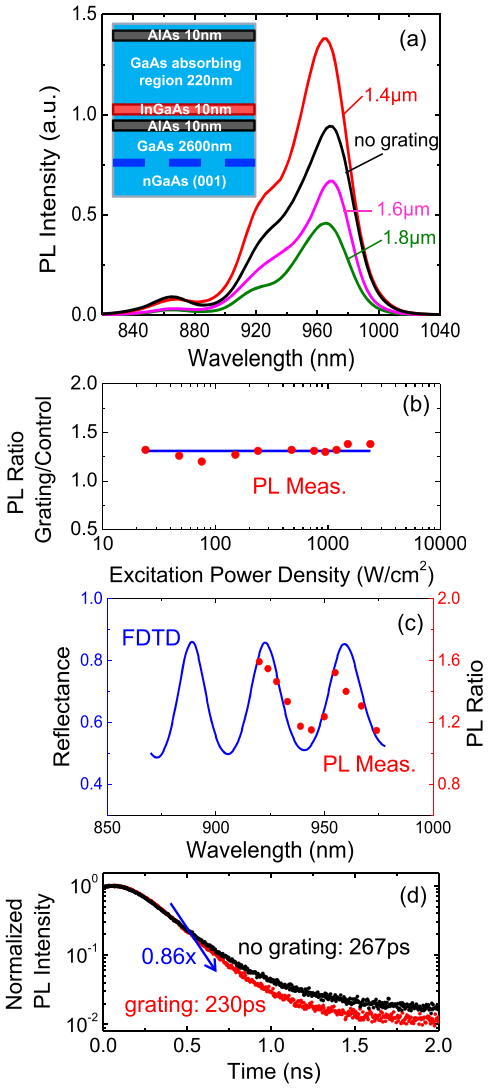

Figure 4. (a) PL response of [010]-aligned planar embedded gratings compared to control. Peak PL of the gratings samples were within 2× of the grating-free control. (b) Excitation-dependent PL performed on the 1.4 μm pitch embedded gratings showed no change compared to control over 2 orders of magnitude of pump-excitation. (c) Temperature-dependent PL (TDPL) performed on the 1.4 μm pitch embedded gratings show distinct changes in peak PL compared to control, forming two distinct oscillations, resulting in 1.2× extraction enhancement. (d) TRPL demonstrating 1.16× decrease in carrier lifetime of the 1.4 μm pitch embedded gratings compared to control, suggesting a modest Purcell enhancement as the second component to emitter enhancement.

intensity. This suggests that the PL increase observed was not pump-dependent and must be associated with other mechanisms.

Next, temperature-dependent PL was performed specifically utilizing red- and blue-shift from temperature-tuning to move the peak InGaAs/GaAs QW emission between 920 and 970 nm to probe any wavelength-related extraction-related mechanisms. As seen in Figure 4c, peak PL emission normalized to control was not constant, but rather forming two distinct peaks over the range of peak emission achieved by the emitter. Specifically, for room-temperature emission at 960 nm, a 1.2× enhancement compared to the floor of the oscillation was observed. More interesting, for emission at 920 and 955 nm, a 1.36× enhancement relative to the floor of the oscillation and a total enhancement of 1.6× compared to control, suggesting that higher enhancement is possible requiring only minor tuning of growth geometry such as grating pitch and fill factor and/or InGaAs/GaAs QW composition to yield further enhancement at room-temperature. Position and magnitude of the two emission peaks were further confirmed by a full-wave analysis using FDTD modeling. Thus, since the control emitter extraction efficiency remains constant to the first order, any differences are suggestive of increased light extraction from the InGaAs/GaAs QW. More specifically, emitter emission that is typically lost to the substrate is instead partially reflected back toward the top surface, increasing net extraction.

While increased light extraction appears to be a primary cause of enhancement in the emitter above embedded 1.4 μm pitch gratings, the floor of the oscillation still remained above the normalized control. Since the extraction is in part a result of resonance between the top surface and embedded silica gratings, the secondary mechanism of enhancement was likely a weak, but significant Purcell effect. To confirm the presence of Purcell effect, time-resolved PL measurements were performed to estimate the carrier lifetime. From this analysis, a 1.16× decrease in carrier lifetime was observed in the emitter above embedded 1.4 μm pitch gratings compared to grating-free control at the peak emission wavelength at room-temperature. As carrier lifetime is inversely proportional to the local optical density of states, this suggests an approximately 1.16× increase in spontaneous emission in the emitter above embedded 1.4 μm pitch gratings compared to control. When accounting for the 1.2× extraction enhancement, the net enhancement totaled 1.4×, nearly exactly the observed enhancement in initial room-temperature PL emission measurement, confirming the enhancement mechanisms as a tandem of extraction and Purcell enhancements.

These studies demonstrate for the first time that a net enhancement to photoluminescence can be achieved from emitters grown seamlessly above embedded silica gratings. It also provides the most sensitive probe of planar coalescence in any homoepitaxial conventional III−V crystal growth technique. As such, not only does this result provide the pathway for high-quality planar coalescence utilizing all-MBE growth approach, but it also unlocks applications requiring the highest level of crystal quality above embedded dielectric microstructures, such as enhanced quantum emitters or low defect III−V heteroepitaxy on silicon. Looking forward, not only is MBE growth presently a viable addition to crystal growth techniques able to achieve embedded dielectric microstructures and planar coalescence, but it also can be leveraged for applications where the highest quality dielectric integration is required, such as monolithic biosensors[36,37] and site-control of quantum emitters.[38−40]

CONCLUSION

We demonstrate for the first time an all-MBE approach to high-quality GaAs planar coalescence over embedded dielectric microstructures. By merging the MBE growth of nonplanar highly selective LEO with planarized growth on corrugated substrates, we successfully formulated of two-stage growth approach that achieved smooth planar coalescence over embedded dielectric microstructures. Specifically, we developed a two-stage growth approach which first uses group-III

DOI: 10.1021/acs.cgd.8b01671
Cryst. Growth Des. 2019, 19, 3085−3091

flux modulated growth to produce a highly selective {011}-faceted lateral epitaxial overgrowth over [010]-aligned silica gratings patterned on (001) substrates, followed by continuous growth to restore the nonplanar LEO template to a smooth (001) surface. Planar coalescence achieved smooth epitaxial layers as low as 3 nm RMS surface roughness and high optical quality with equivalent photoluminescence to grating-free controls. Additionally, in demonstration of the high-quality planar coalescence, we also presented for the first time an intentionally enhanced single quantum well InGaAs/GaAs/AlAs emitter seamlessly grown directly above embedded silica gratings using the two-stage MBE approach, leading to a 1.4× enhancement in photoluminescence as a result of both Purcell and extraction enhancements. Looking forward, the presented all-MBE growth approach to planar coalescence marks a significant advance in the long-standing challenge of seamless integration of high-quality semiconductor epitaxial layers with dielectric microstructures, opening up the potential for important applications, including embedded metasurfaces, enhanced quantum emitters, and an all-MBE approach to metamorphic III−V heteroepitaxy on silicon and other technologically important substrates.

METHODS

Grating Fabrication. For GaAs planar coalescence growth studies, silica gratings were fabricated on (001) GaAs substrates. Fabrication of silica gratings began by depositing 30 nm of silica via plasma-enhanced chemical vapor deposition (PECVD) at 250 °C. Then, high-resolution resist (Futurrex nr9-500p) was used to generate features as small as 0.7 μm using conventional lithography techniques. Using the patterned resist as an etch mask, the PECVD silica was etched using reactive ion etching (RIE) with CHF_3/O_2 chemistry. After the etch, the resist mask was removed and O_2 plasma/HCl digital etch was used to reclaim the episurface after RIE.

MBE Growth. All growth was performed in an EPI Mod Gen II MBE reactor equipped with a buffer and load lock with solid source Ga effusion cell and a valved As cracker. Before growth, fabricated grating samples were cleaned using atomic hydrogen to ensure a clean episurface prior to transfer to the reactor. Once transferred to the growth position, any remaining surface oxides were removed using a 10 min thermal desorption at 600 °C under an As_4 overpressure. First-stage PSE-based LEO was initiated at growth temperatures between 625 and 630 °C under a large As_4 overpressure, 3:1 As_4/Ga flux ratio (76× As_4/Ga BEP ratio), utilizing a 50% PSE duty cycle (30 s growth, then 30 s growth pause) at a growth rate of 0.25 μm/h, as these conditions were sufficient in producing highly selective growth while also maintaining a reasonably high growth rate. After the lateral growth stage was completed, second-stage continuous GaAs growth conditions utilized a 2:1 As_4/Ga flux ratio (45× BEP ratio) with growth temperatures and rates at 570 °C and 0.5 μm/h, respectively.

Structural and Optical Characterization. Planview and cross-sectional SEM were performed using a Zeiss Neon40 FE-SEM. AFM was performed using Veeco Nanoscope V using a silicon probe tip. X-ray rocking curve analysis was performed using a Rigaku SmartLab X-ray diffractometer. Excitation- and temperature-dependent PL was performed using a Nd:YAG laser at 532 nm with excitation up to 2.4 kW/cm^2, 0.5 m grating spectrometer, and a TE-cooled InGaAs detector. Time-resolved PL was performed in a confocal microscope with 495 nm femtosecond pulsed excitation, SPCM detector, and PicoHarp timing.

AUTHOR INFORMATION

Corresponding Authors

*E-mail: daniel.j.ironside@utexas.edu.

*E-mail: sbank@utexas.edu.

ORCID

Daniel J. Ironside: 0000-0002-4555-0845

Notes

The authors declare no competing financial interest.

ACKNOWLEDGMENTS

This work was performed in part at the University of Texas Microelectronics Research Center, a member of the National Nanotechnology Coordinated Infrastructure (NNCI), which is supported by the National Science Foundation (No. ECCS-1542159). This work was also supported by the National Science Foundation (Award No. DMR-1508603 and DMR-1508783). DJI acknowledges support from the National Science Foundation Graduate Fellowship. TAL acknowledges support from the NNCI REU program.

REFERENCES

(1) Huang, Y.-C.; Lin, C.-F.; Chen, S.-H.; Dai, J.-J.; Wang, G.-M.; Huang, K.-P.; Chen, K.-T.; Hsu, Y.-H. InGaN-based light-emitting diodes with an embedded conical air-voids structure. *Opt. Express* **2011**, *19*, A57−A63.

(2) Cho, C.-Y.; Kwon, M.-K.; Park, I.-K.; Hong, S.-H.; Kim, J.-J.; Park, S.-E.; Kim, S.-T.; Park, S.-J. High-efficiency light-emitting diode with air voids embedded in lateral epitaxially overgrown GaN using a metal mask. *Opt. Express* **2011**, *19*, A943−A948.

(3) Birudavolu, S.; Nuntawong, N.; Balakrishnan, G.; Xin, Y. C.; Huang, S.; Lee, S. C.; Brueck, S. R. J.; Hains, C. P.; Huffaker, D. L. Selective area growth of InAs quantum dots formed on a patterned GaAs substrate. *Appl. Phys. Lett.* **2004**, *85*, 2337−2339.

(4) Makhonin, M. N.; Foster, A. P.; Krysa, A. B.; Fry, P. W.; Davies, D. G.; Grange, T.; Walther, T.; Skolnick, M. S.; Wilson, L. R. Homogeneous Array of Nanowire-Embedded Quantum Light Emitters. *Nano Lett.* **2013**, *13*, 861−865.

(5) Noda, S.; Kitamura, K.; Okino, T.; Yasuda, D.; Tanaka, Y. Photonic-Crystal Surface-Emitting Lasers: Review and Introduction of Modulated-Photonic Crystals. *IEEE J. Sel. Top. Quantum Electron.* **2017**, *23*, 1−7.

(6) Nelson, E. C.; Dias, N. L.; Bassett, K. P.; Dunham, S. N.; Verma, V.; Miyake, M.; Wiltzius, P.; Rogers, J. A.; Coleman, J. J.; Li, X.; Braun, P. V. Epitaxial growth of three-dimensionally architectured optoelectronic devices. *Nat. Mater.* **2011**, *10*, 676−681.

(7) Li, J. Z.; Bai, J.; Park, J.-S.; Adekore, B.; Fox, K.; Carroll, M.; Lochtefeld, A.; Shellenbarger, Z. Defect reduction of GaAs epitaxy on Si (001) using selective aspect ratio trapping. *Appl. Phys. Lett.* **2007**, *91*, 021114.

(8) Kataria, H.; Metaferia, W.; Junesand, C.; Zhang, C.; Julian, N.; Bowers, J. E.; Lourdudoss, S. Simple Epitaxial Lateral Overgrowth Process as a Strategy for Photonic Integration on Silicon. *IEEE J. Sel. Top. Quantum Electron.* **2014**, *20*, 380−386.

(9) Nam, O.-H.; Bremser, M. D.; Zheleva, T. S.; Davis, R. F. Lateral epitaxy of low defect density GaN layers via organometallic vapor phase epitaxy. *Appl. Phys. Lett.* **1997**, *71*, 2638−2640.

(10) Nishinaga, T. Microchannel epitaxy: an overview. *J. Cryst. Growth* **2002**, *237−239*, 1410−1417.

(11) Gale, R. P.; McClelland, R. W.; Fan, J. C. C.; Bozler, C. O. Lateral epitaxial overgrowth of GaAs by organometallic chemical vapor deposition. *Appl. Phys. Lett.* **1982**, *41*, 545−547.

(12) Julian, N.; Mages, P.; Zhang, C.; Zhang, J.; Kraemer, S.; Stemmer, S.; Denbaars, S.; Coldren, L.; Petroff, P.; Bowers, J.

DOI: 10.1021/acs.cgd.8b01671
Cryst. Growth Des. 2019, 19, 3085−3091

Coalescence of InP Epitaxial Lateral Overgrowth by MOVPE with V/III Ratio Variation. *J. Electron. Mater.* **2012**, *41*, 845−852.
(13) Astromskas, G.; Wallenberg, L. R.; Wernersson, L.-E. Electrical characterization of thin InAs films grown on patterned Wâ•GaAs substrates. *Journal of Vacuum Science & Technology B: Microelectronics and Nanometer Structures Processing, Measurement, and Phenomena* **2009**, *27*, 2222−2226.
(14) López, M.; Nomura, Y. Surface diffusion length of Ga adatoms in molecular-beam epitaxy on GaAs(100)â€"(110) facet structures. *J. Cryst. Growth* **1995**, *150*, 68−72.
(15) Wang, S. *Lattice Engineering: Technology and Applications*; Pan Stanford, 2012; Chapter 3.
(16) Zytkiewicz, Z. Laterally overgrown structures as substrates for lattice mismatched epitaxy. *Thin Solid Films* **2002**, *412*, 64−75.
(17) Lee, S. C.; Brueck, S. R. J. Nanoscale Patterned Growth Assisted by Surface Out-Diffusion of Adatoms from Amorphous Mask Films in Molecular Beam Epitaxy. *Cryst. Growth Des.* **2016**, *16*, 3669−3676.
(18) Bacchin, G.; Nishinaga, T. A new way to achieve both selective and lateral growth by molecular beam epitaxy: low angle incidence microchannel epitaxy. *J. Cryst. Growth* **2000**, *208*, 1−10.
(19) Lee, S. C.; Malloy, K. J.; Dawson, L. R.; Brueck, S. R. J. Selective growth and associated faceting and lateral overgrowth of GaAs on a nanoscale limited area bounded by a SiO2 mask in molecular beam epitaxy. *J. Appl. Phys.* **2002**, *92*, 6567−6571.
(20) Bacchin, G.; Nishinaga, T. Fabrication of submicrometer structures by PSE/MBE. *J. Cryst. Growth* **2000**, *211*, 389−394.
(21) Nishinaga, T. Microchannel epitaxy: an overview. *J. Cryst. Growth* **2002**, *237*, 1410−1417.
(22) Nishinaga, T.; Bacchin, G. Selective area MBE of GaAs, AlAs and their alloys by periodic supply epitaxy. *Thin Solid Films* **2000**, *367*, 6−12.
(23) Biasiol, G.; Gustafsson, A.; Leifer, K.; Kapon, E. Mechanisms of self-ordering in nonplanar epitaxy of semiconductor nanostructures. *Phys. Rev. B: Condens. Matter Mater. Phys.* **2002**, *65*, 205306.
(24) Horikoshi, Y. Advanced epitaxial growth techniques: atomic layer epitaxy and migration-enhanced epitaxy. *J. Cryst. Growth* **1999**, *201−202*, 150−158.
(25) Sugaya, T.; Okada, Y.; Kawabe, M. Selective growth of GaAs by molecular beam epitaxy. *Jpn. J. Appl. Phys.* **1992**, *31*, L713.
(26) Kawabe, M.; Sugaya, T. Anisotropic Lateral Growth of GaAs by Molecular Beam Epitaxy. *Jpn. J. Appl. Phys.* **1989**, *28*, L1077.
(27) Allegretti, F.; Nishinaga, T. Periodic supply epitaxy: a new approach for the selective area growth of GaAs by molecular beam epitaxy. *J. Cryst. Growth* **1995**, *156*, 1−10.
(28) Fukui, T.; Ando, S. New GaAs quantum wires on 111B facets by selective MOCVD. *Electron. Lett.* **1989**, *25* (2), 410−412.
(29) Takebe, T.; Fujii, M.; Yamamoto, T.; Fujita, K.; Watanabe, T. Orientation-dependent Ga surface diffusion in molecular beam epitaxy of GaAs on GaAs patterned substrates. *J. Appl. Phys.* **1997**, *81*, 7273−7281.
(30) Kapon, E.; Tamargo, M.; Hwang, D. Molecular beam epitaxy of GaAs/AlGaAs superlattice heterostructures on nonplanar substrates. *Appl. Phys. Lett.* **1987**, *50*, 347−349.
(31) Coluci, V.; Cotta, M. Influence of rough substrates on the morphology evolution of epitaxial films. *Phys. Rev. B: Condens. Matter Mater. Phys.* **2000**, *61*, 13703.
(32) Tournié, E.; Ploog, K. H. Surfactant-mediated molecular beam epitaxy of strained layer semiconductor heterostructures. *Thin Solid Films* **1993**, *231*, 43−60.
(33) Pillai, M. R.; Kim, S.-S.; Ho, S. T.; Barnett, S. A. Growth of $In_xGa_{1-x}As$/GaAs heterostructures using Bi as a surfactant. *J. Vac. Sci. Technol., B: Microelectron. Process. Phenom.* **2000**, *18*, 1232−1236.
(34) Tartaglia, J. M.; Crochiere, S. M.; Kalnas, C. E.; Farrington, D. L.; Kronwasser, J. A.; Pearah, P. J. A study of etch pit density and x-ray rocking curves for GaAs substrate evaluation. *J. Electron. Mater.* **1991**, *20*, 345−352.
(35) Yan, Z.; Hamaoka, Y.; Naritsuka, S.; Nishinaga, T. Coalescence in microchannel epitaxy of InP. *J. Cryst. Growth* **2000**, *212*, 1−10.
(36) Misiakos, K.; Kakabakos, S. E.; Petrou, P. S.; Ruf, H. H. A monolithic silicon optoelectronic transducer as a real-time affinity biosensor. *Anal. Chem.* **2004**, *76*, 1366−1373.
(37) Martín-Palma, R. J.; Manso, M.; Torres-Costa, V. Optical biosensors based on semiconductor nanostructures. *Sensors* **2009**, *9*, 5149−5172.
(38) Lee, H.; Johnson, J.; Speck, J.; Petroff, P. Controlled ordering and positioning of InAs self-assembled quantum dots. *J. Vac. Sci. Technol., B: Microelectron. Process. Phenom.* **2000**, *18*, 2193−2196.
(39) Ishikawa, T.; Nishimura, T.; Kohmoto, S.; Asakawa, K. Site-controlled InAs single quantum-dot structures on GaAs surfaces patterned by in situ electron-beam lithography. *Appl. Phys. Lett.* **2000**, *76*, 167−169.
(40) Atkinson, P.; Ward, M.; Bremner, S.; Anderson, D.; Farrow, T.; Jones, G.; Shields, A.; Ritchie, D. Site-control of InAs quantum dots using ex-situ electron-beam lithographic patterning of GaAs substrates. *Jpn. J. Appl. Phys.* **2006**, *45*, 2519.

DOI: 10.1021/acs.cgd.8b01671
Cryst. Growth Des. 2019, 19, 3085−3091